

ARTICLE

Received 28 Aug 2014 | Accepted 21 Feb 2015 | Published 13 Apr 2015

DOI: 10.1038/ncomms7732

Energy transfer pathways in semiconducting carbon nanotubes revealed using two-dimensional white-light spectroscopy

Randy D. Mehlenbacher^{1,*}, Thomas J. McDonough^{1,*}, Maksim Grechko¹, Meng-Yin Wu², Michael S. Arnold³ & Martin T. Zanni¹

Thin film networks of highly purified semiconducting carbon nanotubes (CNTs) are being explored for energy harvesting and optoelectronic devices because of their exceptional transport and optical properties. The nanotubes in these films are in close contact, which permits energy to flow through the films, although the pathways and mechanisms for energy transfer are largely unknown. Here we use a broadband continuum to collect femtosecond two-dimensional white-light spectra. The continuum spans 500 to 1,300 nm, resolving energy transfer between all combinations of bandgap (S_1) and higher (S_2) transitions. We observe ultrafast energy redistribution on the S_2 states, non-Förster energy transfer on the S_1 states and anti-correlated energy levels. The two-dimensional spectra reveal competing pathways for energy transfer, with S_2 excitons taking routes depending on the bandgap separation, whereas S_1 excitons relax independent of the bandgap. These observations provide a basis for understanding and ultimately controlling the photophysics of energy flow in CNT-based devices.

¹Department of Chemistry, University of Wisconsin—Madison, 1101 University Avenue, Madison, Wisconsin 53706, USA. ²Department of Electrical and Computer Engineering, University of Wisconsin—Madison, 1415 Engineering Drive, Madison, Wisconsin 53706, USA. ³Department of Material Science and Engineering, University of Wisconsin—Madison, 1509 University Avenue, Madison, Wisconsin 53706, USA. * These authors contributed equally to this work. Correspondence and requests for materials should be addressed to M.S.A. (email: msarnold@wisc.edu) or to M.T.Z. (email: zanni@chem.wisc.edu).

The performance of electronics, optoelectronics and energy harvesting devices is intimately related to the flow of energy and charge through their respective materials. For example, in nanostructured organic and polymer heterojunction solar cells, excitons photogenerated from solar photons must migrate through a complex energy landscape to the heterointerface where they yield charges that drive electricity¹. The excitons' pathway is determined by the electronic structure of the photovoltaic materials, the site-to-site energetic disorder and the inter-site coupling². Direct and efficient pathways are needed so that excitons can reach the heterointerface before being trapped or annihilated by non-radiative loss mechanisms. Understanding the rates, pathways and bottlenecks is critical to controlling this energy flow and ultimately making better devices.

Semiconducting carbon nanotubes (CNTs) are one candidate for next-generation semiconductor electronics³, near-infrared optoelectronics⁴ and light absorbers or transparent conductors for solar cells⁵. Semiconducting CNTs, with controlled bandgap, can now be purified from their metallic counterparts and fabricated into mesoscale networks of densely interwoven bundles^{6,7}. These films can be used in photovoltaics and photodetectors, in which the semiconducting tubes are photoabsorbers, analogous to electron donor polymers in polymer solar cells⁸. Like polymers, CNTs have large and tunable optical absorption and are solution processable, but nanotubes exhibit ultrafast charge and energy transport over longer distances and are more air stable⁵. While the photophysics of individual nanotubes is an established topic of study^{9,10}, the properties of these new mesoscale films are largely unknown. In addition, the ability to control the bandgap composition of the films makes them a model system for studying exciton and charge transfer. From time-resolved photoluminescence and transient absorption spectroscopy, we know that energy transfers between nanotubes in these films and that excitons can dissociate into free carriers^{11–15}. But the energetic manifold of these coupled thin films is extremely complex, with multiple discrete transitions per nanotube structure and multiple structures of nanotubes per film, resulting in dozens of potential relaxation pathways that are enormously difficult to resolve.

Shown in Fig. 1a is the absorption spectrum for the CNT film that is the focus of this paper and has been used in previously reported prototype photovoltaic devices^{5,16}. It is composed primarily of four different diameter nanotubes, referred to by their (n,m) chiral indices $(7,5)$, $(7,6)$, $(8,6)$ and $(8,7)$. Compared with the absorption spectrum of these nanotubes in solution, the bands are broadened and slightly shifted ($<5\text{ nm}$)^{5,15}, indicating that the nanotube bandgap and photophysics are perturbed when the nanotubes are in close contact. A standard technique to study photophysics of CNTs and other materials is photoluminescence excitation (PLE) spectroscopy, and the PLE spectra of this film, which is shown in Fig. 1b, is similar to those previously reported for other films^{5,17}. Each diameter tube exhibits an S_1 transition in the near-infrared (corresponding to the optical bandgap) and an S_2 transition in the visible. Only two S_2 transitions are observed because the $(7,5)/(7,6)$ and $(8,6)/(8,7)$ transitions overlap. The PLE measurements are performed by scanning an excitation source across the S_2 energy levels while measuring photoluminescence from the S_1 states. The resulting two-dimensional (2D) correlation map reveals the probability for exciton transfer from larger to smaller bandgap nanotubes. However, since there is no time resolution, one cannot distinguish different pathways that lead to the same emission. For example, energy transfer caused by sequential hops from larger to progressively smaller bandgap tubes could produce the same feature in a PLE spectrum as a single 'super-hop' directly to the lowest bandgap tube. Moreover, since energy transfer within

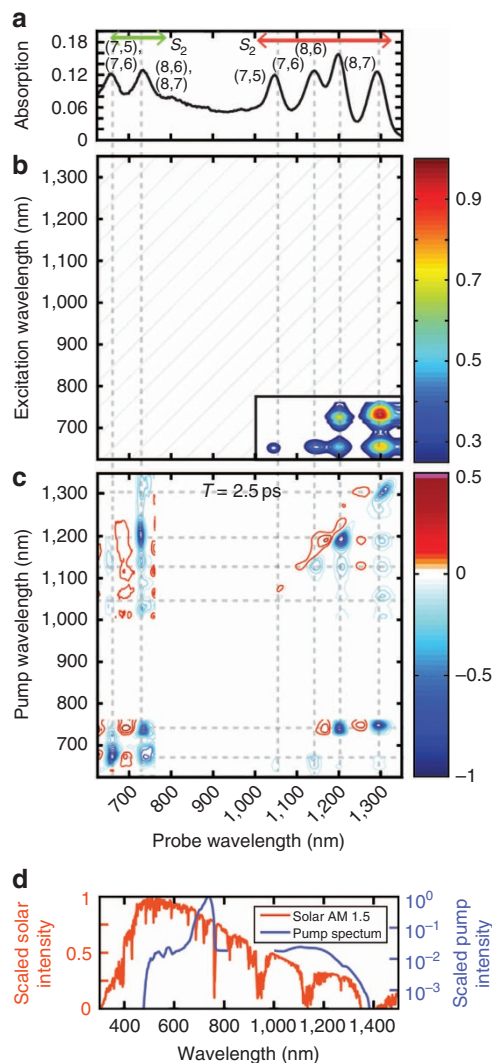


Figure 1 | Spectra of carbon nanotube thin films and white-light laser source. (a) Absorption spectrum, (b) PLE spectrum, (c) 2D white light spectra at pump-probe delay $T = 2,500\text{ fs}$, and (d) log scale pump spectrum compared with the solar spectrum. The sample is composed primarily of four chiralities of nanotubes, each having an S_1 and S_2 transition labelled by their chiral index (n,m) in a. The PLE spectrum is collected as typically done by only pumping the S_2 transition and watching photoluminescence from the S_1 state. Therefore, PLE only measures cross peaks in the S_2/S_1 quadrant. The 2D-WL spectra exhibits cross peaks in all four quadrants. Below the diagonal of the spectrum, the cross peaks are caused by energy transfer. Above the diagonal, the electronic structure intrinsic to the individual nanotubes produces the cross peaks. The intensity of each quadrant is normalized for the sake of visualization. The following figures expand on the features and dynamics measured in each of the individual quadrants. We spectrally filter out the 800 nm bandwidth from our pump, leading to the gap in the spectrum.

the S_2 and the S_1 manifold of states is not measured with PLE spectroscopy, only a fraction of the possible transitions are probed, making it unclear how energy flows from S_2 to S_1 . Characterizing the pathways available for energy flow is critical for designing functional materials.

In this article, we utilize 2D white-light spectroscopy (2D-WL) to study the exciton dynamics in thin films of CNTs. 2D-WL spectroscopy produces a correlation map analogous to PLE spectra, but since it uses a variant of transient absorption

spectroscopy it has femtosecond time resolution¹⁸. We report a version of 2D-WL spectroscopy using a supercontinuum that spans the entire wavelength range of relevance, from 500 to 1,300 nm, and so monitors both the S_1 and S_2 states (see Fig. 1d). The combination of ultrafast time resolution and broad bandwidth enables the kinetics for all possible pathways between all combinations of bright S_1 and S_2 states to be measured. As a result, we obtain a unified mechanism of energy transfer through these materials and observe new photophysics.

Results

2D white-light spectroscopy. Shown in Fig. 1c is a representative 2D-WL spectrum of the same film as measured with PLE spectroscopy (Fig. 1b), but unlike the PLE spectrum the 2D-WL spectrum exhibits peaks in all four quadrants and is time resolved (this spectrum is collected with a 2,500 fs time delay). Each of the transitions in the absorption spectrum creates a pair of diagonal peaks in the 2D-WL spectrum. The negative peak exactly on the diagonal (blue) corresponds to photobleaching of the direct bandgap transition, while the blue-shifted positive peak along the probe axis is from an excited state absorption (red)^{12,19}. In addition to the diagonal peaks, cross peaks appear that correlate different chirality tubes. The 2D-WL spectra are plotted with the probe wavelength along the x -axis and the pump wavelengths along the y -axis so that cross peaks on the lower half of the diagonal correspond to downhill energy transfer. A cut through a specific pump wavelength (along the x -axis) is analogous to the transient absorption spectrum at that wavelength, so that the 2D-WL spectrum can be envisioned as the compilation of a continuous series of transient absorption spectra. However, as explained in the Methods section below, a Fourier transform method is used to measure the pump axis so that all pump frequencies are measured simultaneously and continuously. A continuous frequency axis avoids the one-frequency-at-a-time method of transient absorption that often leads to a piecemeal mapping of the pathways. Moreover, the 2D lineshapes resolve frequency shifts from lineshape changes, which can be difficult to discern in pump-probe spectroscopy. In essence, the 2D-WL spectra provide an instantaneous snapshot of the energy distribution in the photoexcited film.

2D-WL quadrants. Each of the peaks in the 2D-WL spectrum corresponds to a specific combination of pumped and probed states. The combination of energy levels creating each observed peak is given in Supplementary Fig. 8. To simplify the discussion, the PLE and 2D-WL spectra are sectioned into four quadrants corresponding to different combinations of pumping and probing the S_1 and S_2 states. In Fig. 2, we present the 2D-WL spectra for the S_1/S_1 quadrant, that is, we are pumping and probing the S_1 nanotube transition with pump-probe delays of $T=100$, 1,000, and 2,500 fs. These time points were chosen to illustrate the growth of new features. The blue contours correspond to photobleaching, while red contours correspond to photoabsorption. Because there is a residual amount of chirp in our laser pulses (see Supplementary Fig. 3 and Methods), the earliest time point we plot is $T=100$ fs, which we define as our time resolution. A simplified energy diagram is shown to illustrate the pathway that creates each photobleaching peak. Photoabsorption pathways are not marked, but each cross peak has both a photobleach and a corresponding photoabsorption. Cross peaks to phonon side bands are also observed (Supplementary Fig. 8). We plot the kinetics for each of the photobleaching cross peaks (solid lines). To quantify the timescales, the cross peak kinetics are self-consistently fit to a sum of rising and decaying exponentials (Supplementary Methods and Supplementary Table 1)¹¹.

Figures 3 and 4 present 2D-WL spectra for the remaining three quadrants. As in the S_1/S_1 quadrant, diagonal peaks and cross peaks are observed. Each is assigned to a specific pathway (Supplementary Fig. 8). The 2D lineshapes and kinetics differ in all four quadrants, indicating that energy transfer depends on excitation state. We interpret the salient features below.

Photoexcitation transfer between bandgap S_1 states. Each quadrant of the 2D-WL spectra probes photoexcitation transfer among a different class of electronic states. Photoexcitation of S_1 lies below the ionization threshold and so excitons, but not charges, are generated²⁰. All of the cross peaks in this quadrant appear on the lower half of the diagonal, indicating that energy transfer occurs downhill from larger to smaller bandgap tubes. These cross peaks are not seen in the solution samples of uncoupled nanotubes (Supplementary Fig. 5), confirming that they arise from energy transfer. Except for cross peaks to phonon modes (peak X, which grow in after ~ 300 fs and then decay similar to the diagonal peaks), the cross peaks grow in simultaneously, indicating that exciton transfer is equally likely between any downhill combination of nanotubes. Moreover, the cross peaks are round, whereas the diagonal peaks are elongated. The 2D lineshapes of cross peaks measure joint frequency correlations and will appear elongated for correlated frequency distributions²¹. Round cross peaks signify uncorrelated energy transfer, that is, an exciton generated anywhere within the distribution of energies of a particular bandgap nanotube has equal probability of transferring to another nanotube anywhere within the acceptor's distribution of energies. Thus, the inhomogeneity of the bandgap transitions does not impact energy transfer. We quantify these observations by fitting with a simple model using single exponentials (Fig. 2), all of which have time constants between 1 and 3 ps. Taking into account the fitting error, the time constants are indistinguishable. Thus, it is equally likely for an S_1 exciton to relax to the next smallest bandgap as it is to 'super-hop' directly to the smallest bandgap tube. Non-exponential dynamics would be observed if hopping were sequential from large to small bandgap, or presumably if multi-exciton effects were present²². Based on the quality that the data can be fit with single exponentials, the similarity of the transfer rates and a lack of correlation, we conclude that transfer is independent of the spectral overlap, ruling out Förster resonance energy transfer between bright states as the rate limiting mechanism. One possibility is that inter-nanotube energy transfer proceeds through Dexter, exciton tunnelling or another non-Förster mechanism^{23,24}. Another possibility is that inter-nanotube transfer rates are diffusion limited as in previous transient absorption experiments, pumping the S_2 states and probing the S_1 states led to the conclusions that there are 'hot spots' for energy transfer to occur between nanotubes, such as at fibre-fibre intersections, and that diffusion to these 'hot spots' can limit kinetics²⁵. These findings are interesting because previous reports concluded that energy transfer between nanotubes was dominated by a Förster resonance energy transfer process^{13,26}, as one might expect for molecules with such large transition dipoles, whereas we find that energy transfer between nanotubes is limited by a non-resonant process.

Photoexcitation transfer between S_2 states. Photoexcitation transfer also occurs between S_2 states, as revealed by cross peaks appearing within 100 fs in the S_2/S_2 quadrant (Fig. 3, peak C), but the pathways for visible excitation are more complex. Prior work concluded that energy transfer in the S_2 manifold does not take place because of momentum mismatch and fast relaxation to S_1 (~ 40 fs)¹⁴. The 2D-WL spectra clearly show that transfer among

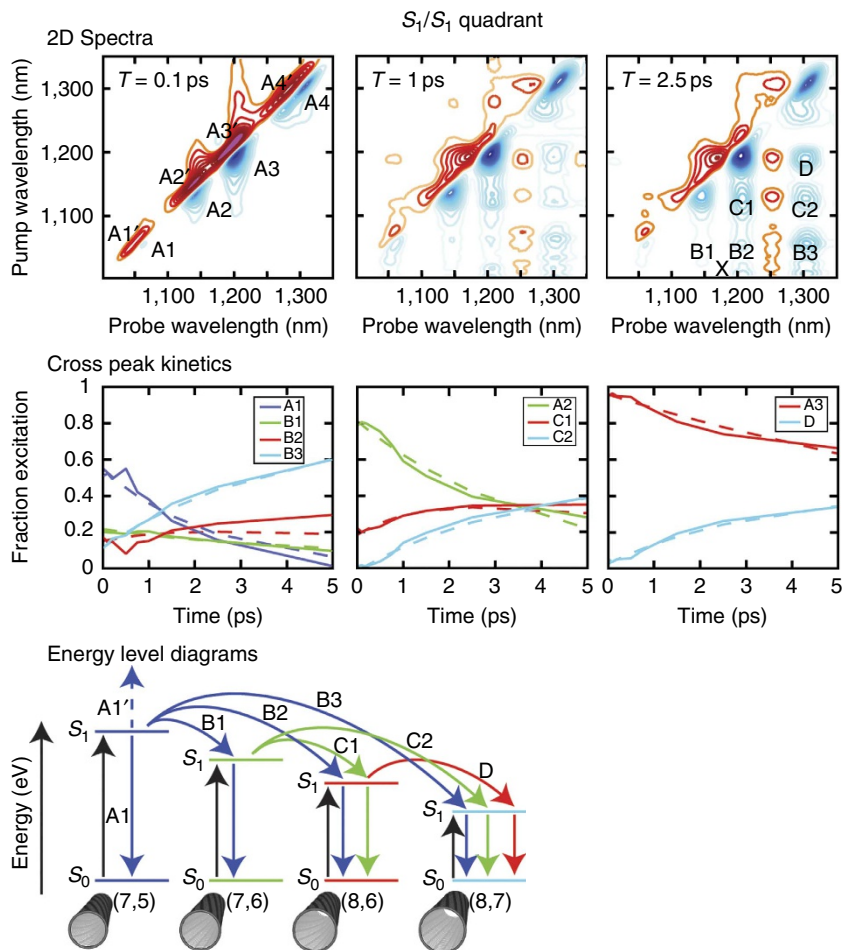


Figure 2 | 2D-WL spectra, kinetics, and energy levels for the S_1/S_1 quadrant. ((a) 2D Spectra) 2D-WL spectra for pump-probe delays $T = 100, 1,000$ and $2,500$ fs. Spectra are normalized to peak A3. The cross peaks are round and grow simultaneously, indicating energy transfer is uncorrelated and independent of bandgap. ((b) Cross peak kinetics) Kinetics of cross peaks used to obtain rates of energy transfer. Kinetics are plotted as fraction of measured photoexcitation to remove lifetime effects. Dashed lines correspond to single exponential fits to data, whose time constants are given in Supplementary Table 1 and are all equal to 1 ps within error. ((c) Energy level diagrams) Energy level diagram showing the energy transfer pathway for each peak in the 2D-WL spectra used to measure the kinetics. Black arrows correspond to pumped transitions. Blue, green, and red arrows correspond to excitons that were initially excited on (7,5), (7,6) and (8,6) nanotubes, respectively. Dashed arrows correspond to excited state absorption, solid arrows correspond to ground state bleaches/stimulated emission and curved arrows correspond to energy transfer. More complete energy level diagrams are given in Supplementary Fig. 6 for all of the peaks seen in the 2D-WL spectrum.

S_2 states is fast enough to compete with relaxation to S_1 , enabling energy redistribution on the S_2 manifold. Thus, energy transfer on both the S_2 and S_1 states are contributing to the features observed in the PLE spectra.

Due to the degeneracies, the S_2/S_2 quadrant only resolves energy transfer between (7,5/6) to (8,6/7) tubes. However, the remaining S_2 pathways can be monitored in the S_2/S_1 quadrant because the S_1 transitions are all well-resolved (Fig. 3). Based on the frequencies of the peaks (dashed lines), the S_2 transitions of the (7,5) and (7,6) tubes are at 654 nm and 656 nm, respectively, while the (8,6) and (8,7) tubes are at 731 nm and 750 nm, respectively. Interestingly, cross peaks are observed both above and below the diagonal of this quadrant, as marked by cross peaks H and H'. H and H' indicate energy transfer from (8,6) to (8,7) as well as from (8,7) to (8,6), in contrast to S_1 energy transfer in which only the former process occurs. From these features we conclude that the near degeneracy of the S_2 states of the (8,6) and (8,7) tubes enables energy transfer to occur in either direction. Moreover, energy transfer between these nearly degenerate states is extremely fast, because unlike any other peaks in the 2D-WL

spectra (other than the phonon side bands), peaks H and H' are already very intense at $T = 100$ and do not appreciably grow in intensity with time delay. Thus, 100 fs is an upper bound for transfer between S_2 states. Other pathways that might contribute to these peaks are eliminated by examining other quadrants, for example, these peaks could be generated by S_2 relaxation to S_1 followed by inter-nanotube transfer among S_1 states, but this pathway is ruled out because the S_1/S_1 quadrant cross peaks appear in picoseconds not femtoseconds. An interesting consequence of the S_2 dynamics is that visible S_2 excitation of an (8,7) tube can transfer to an (8,6) tube before relaxing to S_1 , resulting in a pathway that deposits more energy on the S_1 state of the (8,6) tube than if the (8,7) S_1 bandgap transition was irradiated directly. Similar conclusions are drawn for transitions between the (7,5) and (7,6) tubes, although the cross peaks are not as well-resolved (appearing as shoulders) because these transitions are more closely spaced. Not all downhill pathways are observed. We see no evidence for relaxing directly from the S_2 state of one nanotube to the S_1 state of another, which is energetically downhill (grey transitions in Fig. 3, peaks K and M). Peaks I and J

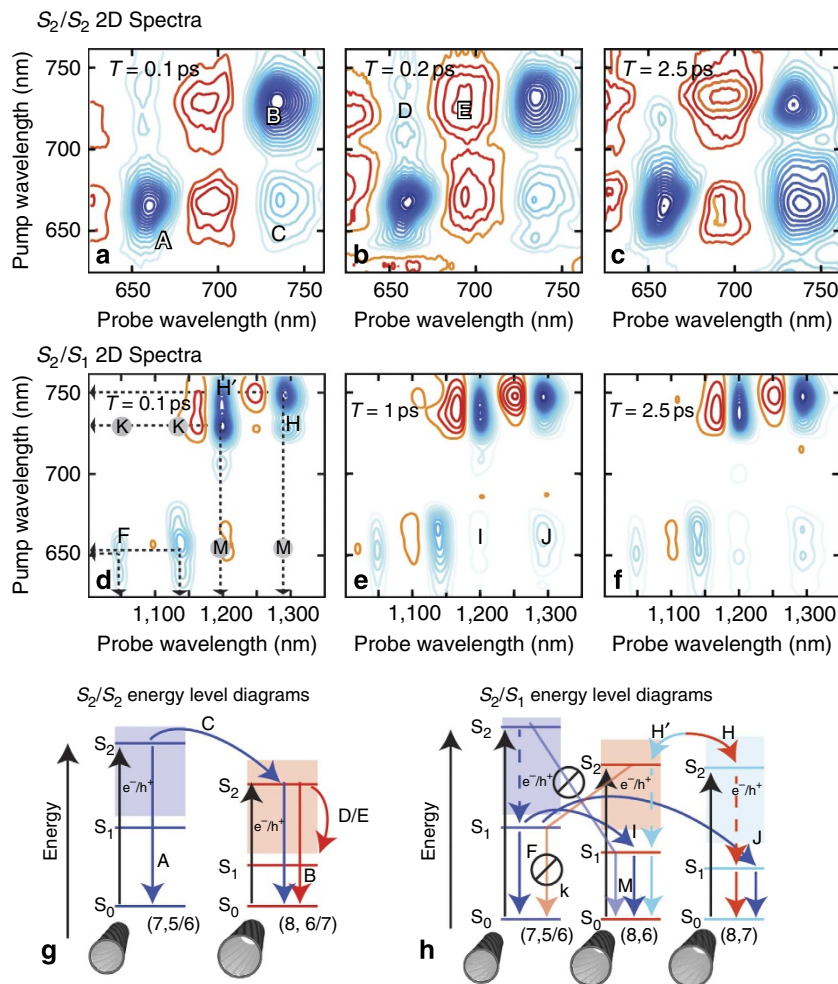


Figure 3 | 2D-WL spectra and energy levels for the S_2/S_2 and S_2/S_1 quadrants. 2D-WL spectra of the S_2/S_2 quadrant for pump-probe delays (a) $T = 100$ fs, (b) $T = 200$ fs and (c) $T = 2,500$ fs, normalized to peak A. Cross peaks indicate that energy transfers between nanotubes on their S_2 states. The cross peaks appear at much earlier time delays than in the S_1/S_1 quadrant, indicating much faster energy transfer. Normalized 2D-WL spectra of the S_2/S_1 quadrant for (d) $T = 100$ fs, (e) $T = 1,000$ fs and (f) $T = 2,500$ fs. This quadrant resolves energy transfer between the degenerate S_2 states. Cross peaks H and H' indicate that energy transfers both from (8,7) to (8,6) as well from (8,6) to (8,7), which is not observed in the S_1 states. ((g) and (h) Energy level diagrams) Schematic energy levels and energy transfer pathways labelled by their corresponding peaks in the 2D-WL spectra. Blue, red and cyan arrows correspond to excitons that have been initially excited on the (7,5/6), (8,6) and (8,7) nanotubes, respectively. Dashed arrows correspond to relaxation between energy manifolds and curved arrows correspond to energy transfer. Cross peaks K and M are where we would expect to see signal if excitons hop directly from the S_2 state of one nanotube to the S_1 state of another.

cannot result from this pathway because the lifetime of the S_2 state is ~ 40 fs¹⁴, but these cross peaks are not observed until ~ 1 ps, which corresponds to the time scale for energy transfer on the S_1 manifold. Apparently, coupling between S_1 and S_2 states on different nanotubes is not large enough to activate this pathway. Thus, intertube energy transfer occurs among S_2 states and among S_1 states, but only intratube transfer connects the two manifolds.

Possible signatures of charge transfer. Besides exciton transfer, we also observe features that we believe are due to charge generation. In the S_2/S_2 quadrant, weak cross peaks are observed on the upper half of the spectrum (peaks D and E). These peaks cannot be caused by uphill energy transfer because the energy difference between (7,5/6) and (8,6/7) S_2 states is $\gg kT$ nor can they be caused by direct relaxation from S_2 to S_1 of different bandgap tubes, which is a process ruled out in the previous paragraph. An alternative hypothesis is that peaks D and E originate from a Stark shift arising from free carrier generation. We

estimate that the electric field necessary to produce this shift would be ~ 87 V μm^{-1} , which is consistent with other reported electric field-induced shifts in CNTs^{27,28}. This hypothesis is supported because peaks D and E in the S_2/S_2 quadrant have no equivalent features in other quadrants and it is known that the S_2 excitation overlaps the free carrier continuum, whereas the S_1 states are too low in energy to generate free carriers²⁷. Photogenerated free carriers on (8,6/7) nanotubes could perturb the S_2 of nearby (7,5/6) nanotubes, Stark shifting the electronic states to yield a photoabsorption and photobleach, as previously assigned using transient absorption spectroscopy^{12,29}. The free carrier signals are much weaker than the exciton peaks, which is consistent with prior work that showed charge generation is a minority process^{12,30}. Unlike pump-probe measurements, these 2D-WL cross peaks have no other overlapping features and so are background free, allowing the free carrier dynamics to be resolved at very early time delays. Auger ionization has also been shown to produce free carriers³¹, however based on our signal intensity, we believe that we are in a regime where most nanotubes have a single exciton initially excited (see Supplementary discussion)³⁰.

Auger ionization should also yield free carriers through S_1 excitation, but this is not observed.

Anti-correlated electronic states. Other interesting features appear in the S_1/S_2 quadrant (Fig. 4). We observe cross peaks between S_1 and S_2 states of the same but not different chirality tubes. These cross peaks cannot be due to exciton transfer, because pumping S_1 is too low in energy to transfer to S_2 . Instead, these cross peaks are measuring the electronic correlation internal to the nanotubes. In other words, they arise because the S_1 and S_2 electronic states are not perfectly orthogonal¹⁹. The centre line slopes are negative and elongated perpendicular to the diagonal (the dashed line is a visual guide), which indicates that the S_1 and S_2 transitions are anti-correlated. Anticorrelation means that large S_2 transitions are correlated with small S_1 bandgaps and *vice versa* for a given (n,m) nanotube (Supplementary Fig. 8) (no correlation would produce round cross peaks). For nanotubes dispersed in solution, we only observe weak anticorrelation (Supplementary Fig. 7), leading us to conclude that the anticorrelation in energy levels is caused by the film casting. Stranks *et al.*³² observed anti-correlated peak shifts in CNT absorption and emission spectra for nanotubes wrapped with rigid porphyrin molecules (but not for PFO wrapping as in our samples), which they attributed to localized strain of the nanotube. Alternative theories for the anti-correlated lineshape are considered in the Supplementary discussion, but it appears that strain caused by surface tension during film casting, differences in thermal expansion (our films are annealed) or mechanical stress on the nanotubes lowers the S_1 while raising the S_2 energy gap (and *vice versa*).

2D lineshapes measure spectral diffusion. 2D-WL spectroscopy also probes dynamics through the time evolution of the 2D lineshapes. The elongation of the diagonal peaks measures the distribution of energies that the bandgap can span for each particular (n,m) nanotube, that is, the inhomogeneity of the bandgap transitions³³. Thus, the peak elongation along the diagonal is a measure of the energetic disorder in the film. In all quadrants, the peak shapes become rounder with time delay, indicating spectral diffusion. Spectral diffusion could be caused by the diffusion of excitons as they sample different environments along the tube lengths, by relaxation of the dielectric on exciton formation³³, or by energy transfer among nanotubes of the same chirality. Measuring the kinetics of the 2D peak shapes probes the dynamics of these processes³³. Thus, after ~ 2 ps when the

peaks are mostly round, the excitons have fully sampled the available environment. We point out that, on the larger bandgap nanotubes, the peaks are still elongated along the diagonal after 2 ps. We believe that this long-lived inhomogeneity is a signature of trapped excitons, because trapped excitons would not be able to fully sample the potential energy landscape. Experiments are underway to contrast the 2D lineshapes of coupled and uncoupled nanotubes to test this hypothesis and better understand the effects of nanotube couplings.

Discussion

Using 2D-WL spectroscopy, we have resolved all possible pathways for energy transfer that can be optically probed in this CNT thin film. The bird's-eye view of a 2D-WL spectrum provides an unprecedented level of clarity because of the continuous and broad wavelength range combined with femto-second time resolution. In many instances, unambiguous peak assignments required self-consistent checks between multiple quadrants, which are not often reported with standard transient absorption spectroscopy. We found that all pathways are equally likely on the S_1 manifold, indicating that Förster energy transfer is not the rate limiting step for exciton transfer. Energy transfer on the S_2 manifold is 10 times faster and can transfer on sub-100 fs timescales between degenerate tubes. As a result, redistribution between S_2 states competes with relaxation to the S_1 states, producing more complex pathways for excitons created from visible than infrared light. These principles will be useful for guiding the design of mesoscale thin films of semiconducting CNTs used in photovoltaics and other optoelectronics.

Methods

Sample preparation. The procedure used to prepare semiconducting CNTs is adopted from Nish *et al.*⁶ and is described in more detail in the Supplementary Methods. It uses poly(9,9-dioctylfluorenyl-2,7-diyl) (PFO, American Dye Source) mixed with high pressure carbon monoxide (HiPco) single-wall CNT mud (NanoIntegris) (5.3% carbon by weight) to selectively purify the semiconducting nanotubes from the metallic tubes and impurities using ultracentrifugation. Once purified, excess PFO is removed, resulting in a CNT:PFO solution with a weight ratio of 1:2 that is used to drop cast a film on a 1 in \times 1 in substrate of indium tin oxide on glass. The resulting CNT film is annealed at 150 °C for 30 min under N_2 atmosphere to remove any residual solvent and encapsulated with an epoxied cover slip to exclude oxygen. Prior to 2D-WL measurements, photoluminescence emission spectra (Horiba Scientific NanoLog FluoroLog3) are collected to confirm that energy transfer is observed within the films (Fig. 1b and Supplementary Fig. 1).

2D-WL spectrometer. There are many different spectrometer designs for collecting 2D spectra^{18,34–42}. Our spectrometer design, shown in Supplementary Fig. 2 and described more fully in the Supplementary Methods, is very similar to a transient absorption spectrometer. The main difference is that the pump pulse has been shaped into a pair of collinear pulses using birefringent wedges⁴³. Alternatively, one can use an interferometer^{37,44} or pulse shaper^{45,46} to create the pulse pairs. To generate the white-light continuum, $< 1 \mu\text{J}$ from the output of a Ti:Sapphire regenerative amplifier (800 nm, 150 fs, 1 kHz) is focused into each of two YAG crystals that are 4-mm thick⁴⁷. A representative pump spectrum is shown in Fig. 1d and compared with the solar spectrum. To limit pulse broadening, the optical path for the white light of the probe only uses reflective optics. For the pump beam, the white light must pass through the birefringent wedges, and so we compensate for pump dispersion using a prism compressor. Because of the large bandwidth of our optical pulses (~ 250 THz), the wedges introduce a significant dispersion to our pulses and so prisms cannot compress the entire bandwidth at once. As a result, the 2D-WL spectra are collected in two halves, with the pump pulses either compressed for the S_1 or the S_2 transition. Optical Kerr effect cross-correlations using the 800 nm laser pulses in CaF_2 are used to measure the group delay of the pump and probe pulses (Supplementary Fig. 3), which sets our time resolution to < 150 fs for either wavelength range. We also use the prism compressor to filter out the fundamental 800 nm light, although there are no resonant transitions in these samples at 800 nm. To make sure that the pump pulse is only creating one exciton per nanotube, the white light is defocused to an intensity that only produces approximately one exciton per 400 nm, which corresponds to the average length of the CNTs. A number of control experiments are presented in the Supplementary Discussion to support this conclusion.

To collect the 2D data, the time delay between the pair of pump pulses is scanned while measuring the spectrum of the probe. To generate the pump axis of the 2D

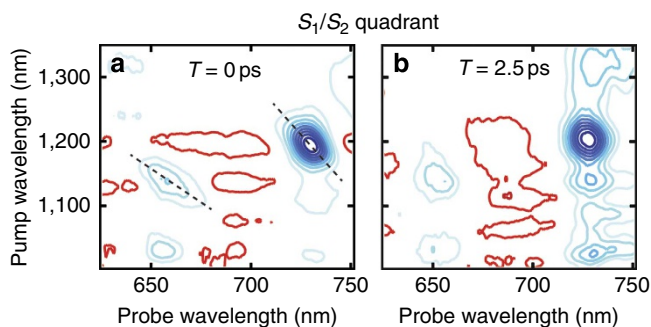


Figure 4 | 2D-WL spectra of the S_1/S_2 quadrant. 2D-WL spectra of the S_1/S_2 quadrant for (a) $T = 0$ and (b) 2,500 fs. These cross peaks are not caused by energy transfer, but result from a change in the S_2 electronic state by pumping the S_1 state. The cross peaks are elongated anti-diagonally, indicating an anticorrelation in the frequency distribution of the S_1 and S_2 states. Dashed lines are guides to the eye to highlight the anti-correlated lineshapes of the cross peaks.

spectrum, the data are Fourier transformed and phased according to the projection slice theorem⁴⁸. The Fourier transform separates out all of the frequency components spanned by the pump bandwidth, analogous to scanning a continuous series of narrowband pump pulses such as with a NOPA. Vertical lines in the spectra are due to tails of the Lorentzian lineshapes. Horizontal tails are not as prominent because of destructive interference of the bleach and excited state absorption²¹.

References

- Lanzani, G. *The Photophysics behind Photovoltaics and Photonics* (Wiley, John & Sons, Inc., 2012).
- Athanasopoulos, S., Emelianova, E. V., Walker, A. B. & Beljonne, D. Exciton diffusion in energetically disordered organic materials. *Phys. Rev. B* **80**, 195209 (2009).
- Wang, C., Takei, K., Takahashi, T. & Javey, A. Carbon nanotube electronics—moving forward. *Chem. Soc. Rev.* **42**, 2592–2609 (2013).
- Avouris, P., Freitag, M. & Perebeinos, V. Carbon-nanotube photonics and optoelectronics. *Nat. Photonics* **2**, 341–350 (2008).
- Arnold, M. S. *et al.* Recent developments in the photophysics of single-walled carbon nanotubes for their use as active and passive material elements in thin film photovoltaics. *Phys. Chem. Chem. Phys.* **15**, 14896–14918 (2013).
- Nish, A., Hwang, J. Y., Doig, J. & Nicholas, R. J. Highly selective dispersion of single-walled carbon nanotubes using aromatic polymers. *Nat. Nanotechnol.* **2**, 640–646 (2007).
- De Volder, M. F., Tawfick, S. H., Baughman, R. H. & Hart, A. J. Carbon nanotubes: present and future commercial applications. *Science* **339**, 535–539 (2013).
- Shea, M. J. & Arnold, M. S. 1% solar cells derived from ultrathin carbon nanotube photoabsorbing films. *Appl. Phys. Lett.* **102**, 243101 (2013).
- Carlson, L. J. & Krauss, T. D. Photophysics of individual single-walled carbon nanotubes. *Acc. Chem. Res.* **41**, 235–243 (2008).
- Ma, Y.-Z., Hertel, T., Vardeny, Z. V., Fleming, G. R. & Valkunas, L. *Ultrafast Spectroscopy of Carbon Nanotubes, in Carbon Nanotubes: New Topics in the Synthesis, Structure, Properties and Application.* in (eds Dresselhaus, M. S., Dresselhaus, G. & Jorio, A.) 111, 321–352 (Springer, Berlin, 2008).
- Koyama, T. *et al.* Bright luminescence and exciton energy transfer in polymer-wrapped single-walled carbon nanotube bundles. *J. Phys. Chem. Lett.* **1**, 3243–3248 (2010).
- Soavi, G. *et al.* Ultrafast charge photogeneration in semiconducting carbon nanotubes. *J. Phys. Chem. C* **117**, 10849–10855 (2013).
- Lefebvre, J. & Finnie, P. Photoluminescence and Forster resonance energy transfer in elemental bundles of single-walled carbon nanotubes. *J. Phys. Chem. C* **113**, 7536–7540 (2009).
- Luer, L., Crochet, J., Hertel, T., Cerullo, G. & Lanzani, G. Ultrafast excitation energy transfer in small semiconducting carbon nanotube aggregates. *ACS Nano* **4**, 4265–4273 (2010).
- Mehlenbacher, R. D. *et al.* Photoexcitation dynamics of coupled semiconducting carbon nanotube thin films. *Nano Lett.* **13**, 1495–1501 (2013).
- Bindl, D. J., Shea, M. J. & Arnold, M. S. Enhancing extraction of photogenerated excitons from semiconducting carbon nanotube films as photocurrent. *Chem. Phys.* **413**, 29–34 (2013).
- Bachilo, S. M. *et al.* Structure-assigned optical spectra of single-walled carbon nanotubes. *Science* **298**, 2361–2366 (2002).
- Hamm, P. & Zanni, M. *Concepts and Methods of 2D Infrared Spectroscopy* (Cambridge Univ. Press, 2011).
- Zhu, Z. *et al.* Pump-probe spectroscopy of exciton dynamics in (6,5) carbon nanotubes. *J. Phys. Chem. C* **111**, 3831–3835 (2007).
- Wang, F., Dukovic, G., Brus, L. E. & Heinz, T. F. The optical resonances in carbon nanotubes arise from excitons. *Science* **308**, 838–841 (2005).
- Ge, N.-H., Zanni, M. T. & Hochstrasser, R. M. Effects of vibrational frequency correlations on two-dimensional infrared spectra. *J. Phys. Chem. A* **106**, 962–972 (2002).
- Graham, M. W. *et al.* Exciton dynamics in semiconducting carbon nanotubes. *J. Phys. Chem. B* **115**, 5201–5211 (2011).
- Olaya-Castro, A. & Scholes, G. D. Energy transfer from Förster–Dexter theory to quantum coherent light-harvesting. *Int. Rev. Phys. Chem.* **30**, 49–77 (2011).
- Wong, C. Y., Curutchet, C., Tretiak, S. & Scholes, G. D. Ideal dipole approximation fails to predict electronic coupling and energy transfer between semiconducting single-wall carbon nanotubes. *J. Chem. Phys.* **130**, 081104 (2009).
- Grechko, M. *et al.* Diffusion-assisted photoexcitation transfer in coupled semiconducting carbon nanotube thin films. *ACS Nano* **8**, 5383–5394 (2014).
- Yang, J. *et al.* Photoluminescence from exciton energy transfer of single-walled carbon nanotube bundles dispersed in ionic liquids. *J. Phys. Chem. C* **116**, 22028–22035 (2012).
- Crochet, J. *et al.* Free-carrier generation in aggregates of single-wall carbon nanotubes by photoexcitation in the ultraviolet regime. *Phys. Rev. Lett.* **107**, 257402 (2011).
- Mohite, A. D., Gopinath, P., Shah, H. M. & Alphenaar, B. W. Exciton dissociation and stark effect in the carbon nanotube photocurrent spectrum. *Nano Lett.* **8**, 142–146 (2008).
- Crochet, J. *et al.* Free-carrier generation in aggregates of single-wall carbon nanotubes by photoexcitation in the ultraviolet regime. *Phys. Rev. Lett.* **107**, 257402 (2011).
- Dowgiallo, A. M., Mistry, K. S., Johnson, J. C. & Blackburn, J. L. Ultrafast spectroscopic signature of charge transfer between single-walled carbon nanotubes and C60. *ACS Nano* **8**, 8573–8581 (2014).
- Yuma, B. *et al.* Biexciton, single carrier, and trion generation dynamics in single-walled carbon nanotubes. *Phys. Rev. B* **87**, 205412 (2013).
- Stranks, S. D., Sprafke, J. K., Anderson, H. L. & Nicholas, R. J. Electronic and mechanical modification of single-walled carbon nanotubes by binding to porphyrin oligomers. *ACS Nano* **5**, 2307–2315 (2011).
- Graham, M. W., Ma, Y. Z., Green, A. A., Hersam, M. C. & Fleming, G. R. Pure optical dephasing dynamics in semiconducting single-walled carbon nanotubes. *J. Chem. Phys.* **134**, 034504 (2011).
- Tekavec, P. F., Myers, J. A., Lewis, K. L. M. & Ogilvie, J. P. Two-dimensional electronic spectroscopy with a continuum probe. *Opt. Lett.* **34**, 1390–1392 (2009).
- Engel, G. S. *et al.* Evidence for wavelike energy transfer through quantum coherence in photosynthetic systems. *Nature* **446**, 782–786 (2007).
- Harel, E., Fidler, A. F. & Engel, G. S. Real-time mapping of electronic structure with single-shot two-dimensional electronic spectroscopy. *Proc. Natl Acad. Sci. USA* **107**, 16444–16447 (2010).
- DeFlores, L. P., Nicodemus, R. A. & Tokmakoff, A. Two-dimensional Fourier transform spectroscopy in the pump-probe geometry. *Opt. Lett.* **32**, 2966–2968 (2007).
- Stone, K. W. *et al.* Two-quantum 2D FT electronic spectroscopy of biexcitons in GaAs quantum wells. *Science* **324**, 1169–1173 (2009).
- Aeschlimann, M. *et al.* Coherent two-dimensional nanoscopy. *Science* **333**, 1723–1726 (2011).
- Nardin, G., Autry, T. M., Silverman, K. L. & Cundiff, S. T. Multidimensional coherent photocurrent spectroscopy of a semiconductor nanostructure. *Opt. Express* **21**, 28617–28627 (2013).
- Turner, D. B., Arpin, P. C., McClure, S. D., Ulness, D. J. & Scholes, G. D. Coherent multidimensional optical spectra measured using incoherent light. *Nat. Commun.* **4**, 2298 (2013).
- Selig, U. *et al.* Inherently phase-stable coherent two-dimensional spectroscopy using only conventional optics. *Opt. Lett.* **33**, 2851–2853 (2008).
- Brida, D., Manzoni, C. & Cerullo, G. Phase-locked pulses for two-dimensional spectroscopy by a birefringent delay line. *Opt. Lett.* **37**, 3027–3029 (2012).
- Helbing, J. & Hamm, P. Compact implementation of Fourier transform two-dimensional IR spectroscopy without phase ambiguity. *J. Opt. Soc. Am. B* **28**, 171–178 (2010).
- Shim, S. H. & Zanni, M. T. How to turn your pump-probe instrument into a multidimensional spectrometer: 2D IR and Vis spectroscopies via pulse shaping. *Phys. Chem. Chem. Phys.* **11**, 748–761 (2009).
- Shim, S.-H., Strasfeld, D. B. & Zanni, M. T. Generation and characterization of phase and amplitude shaped femtosecond mid-IR pulses. *Opt. Express* **14**, 13120–13130 (2006).
- Bradler, M., Baum, P. & Riedle, E. Femtosecond continuum generation in bulk laser host materials with sub- μ J pump pulses. *Appl. Phys. B* **97**, 561–574 (2009).
- Brixner, T., Mancal, T., Stiopkin, I. V. & Fleming, G. R. Phase-stabilized two-dimensional electronic spectroscopy. *J. Chem. Phys.* **121**, 4221–4236 (2004).

Acknowledgements

This work was supported by the Air Force Office of Scientific Research (FA9550-12-1-0063) and by the NSF through the University of Wisconsin–Madison Center of Excellence for Materials Research and Innovation award DMR-1121288. R.D.M. is supported by the Department of Defense, the Air Force Office of Scientific Research, the National Defense Science and Engineering Graduate (NDSEG) Fellowship, 32 CFR 168a. T.J.M. is supported by the NSF Graduate Research Fellowship Program (DGE-1256259).

Author contributions

All authors designed the research. R.D.M. and T.J.M. performed the research. R.D.M. analysed the data. M.-Y.W. prepared the samples. R.D.M., M.S.A. and M.T.Z. wrote the manuscript.

Additional information

Supplementary Information accompanies this paper at <http://www.nature.com/naturecommunications>

Competing financial interests: M.T.Z. is an owner of PhaseTech Spectroscopy, Inc.

Reprints and permission information is available online at <http://npg.nature.com/reprintsandpermissions/>

How to cite this article: Mehlenbacher, R. D. *et al.* Energy transfer pathways in semiconducting carbon nanotubes revealed using two-dimensional white-light spectroscopy. *Nat. Commun.* 6:6732 doi: 10.1038/ncomms7732 (2015).